ISSN (Print) 1226-1750
ISSN (Online) 2233-6656
Journal of Magnetics 27(4), 335-340 (2022) https://doi.org/10.4283/JMAG.2022.27.4.335

Field-driven Modulation of Spin Hall Magnetoresistance in Nanoscale-layered Pt/$IrMn_3$/NiFe Heterostructures

Nga T. Do[1,2], Thi Kim Hang Pham[1,3], Seung Young Park[4], and Tae Hee Kim[1]*

[1]*Department of Physics, Ewha Womans University, Seoul 03760, Republic of Korea*
[2]*IBS Center for Quantum Nanoscience, Ewha Womans University, Seoul 03760, Republic of Korea*
[3]*Department of Materials Technology, Faculty of Applied Sciences, HCMC University of Technology and Education, Ho Chi Minh City 700000, Vietnam*
[4]*Korea Basic Science Institute, Daejeon 34133, Republic of Korea*

(Received 12 October 2022, Received in final form 25 October 2022, Accepted 26 October 2022)

Spin Hall magnetoresistance (SMR) emerges from both spin Hall effect (SHE) and inverse spin Hall effect (ISHE), which is usually investigated in a nonmagnetic heavy metal (NM) in contact with a ferromagnet (FM). Depending on the orientation of FM magnetization and spin polarization of NM layer, the transmission or reflection of the spin current at the FM\NM interface could occur. SMR was investigated in 1.5 nm NiFe\3.0 nm $IrMn_3$\3.0 nm Pt magnetic heterostructures. $IrMn_3$ thin film grown on ferromagnetic NiFe layer exhibits the glassy magnetic behavior and displays spin reorientation transition in the magnetic field-temperature space. Below the Néel temperature of $IrMn_3$, the angle dependence of MR measurement in the *xy* and *xz* plane showed a normal positive SMR. However, a sign change in SMR was observed in the magnetic field applied in the *yz* plane. The switching from negative to positive SMR occurs at the field above a critical value of 6 kG. Our results provide a potential advantage for the source of spin flow in the signal in multilayer heterostructures and highlight the importance of magnetic structure (Néel vector) in AF, which opens the possible way to manipulate the spin current transportation and AF memory devices.

Keywords : spin Hall magnetoresistance, antiferromagnets, Néel order, magnetic heterostructures, tunability

1. Introduction

Antiferromagnets (AFM) have received tremendous attention in the past decade because of their promising applications for next-generation innovative devices, based on various advantages such as their fast dynamics and high robustness against magnetic field fluctuation [1, 2]. Now, perpendicular stacks involving heavy metals (HM) and ferromagnetic transition metals (or insulators) reveal a peculiar interface-sensitive phenomenon usually known under the broad name of spin Hall magnetoresistance (SMR). This effect is described as a sizable anisotropic magnetoresistance (MR) that depends on the angle between the magnetization and the direction transverse to the current flow [3]. The amplitude of SMR is defined as the resistive difference between the perpendicular ($\rho_\perp$) and parallel ($\rho_\parallel$) configuration of spin current polarization relative to the magnetic order of magnetic layers:

$$\rho_{SMR} = \rho_\parallel - \rho_\perp. \quad (1)$$

Experimental studies of SMR have explored the different combinations of HM and ferromagnetic insulators (FI) (or metals). In general, positive SMR ($\rho_{SMR} > 0$) is predicted for HM/FI bilayer structures, the FI absorbs more spin current when an applied field (H) is parallel to an in-plane charge current. Recently, the research reported to date on SMR has been extended to AFM, after the signatures of spin-orbit torques (SOT) were reported in antiferromagnetic (AF) bilayer systems [4-6]. In bilayers of AFM and HM, as long as the magnetic order parameter can be defined in AFM, the SMR effects similar to their ferromagnetic counterpart were reported by several theoretical and experimental works [7, 8].

In the case of NiO inserted between Pt/YIG, the negative SMR competes with the conventional positive SMR contribution from YIG, as the thickness of NiO increases. In Hou *et al.*'s earlier report, the anomalous negative SMR at low temperature (T) was attributed to a

©The Korean Magnetics Society. All rights reserved.
*Corresponding author: Tel: +82-2-3277-4647
e-mail: taehee@ewha.ac.kr

© 2022 Journal of Magnetics

spin-flop configuration whereby Néel order of the NiO is perpendicularly coupled to the magnetization (M) of YIG [9]. The SMR has also been reported in metallic AF (FeMn)/HM (Pt). It is unclear the role of FeMn in SMR effects in the metallic bilayers, since FeMn presents a residual magnetization [10]. The strong dependence of SMR effects on the thickness of FeMn (t_{FeMn}), in other words the spin configuration of FeMn was reported. For $t_{FeMn} < 3$ nm, the significant amounts of uncompensated spins in the FeMn layer can be rotated easily by the external field. However, recently theoretical and experimental works have been also provided a framework for understanding the anomalous Hall effect using Berry-phase concepts [11]. Nevertheless, it is generally known that passive AFM insertion-layers could play a key role in pinning the FM layers (or FM and HM layers) in spintronic devices. Therefore, one can expect the effective tunability of SMR signal in FI/AFM insulator/HM hybrid SMR devices. Finally, an interesting issue that remains to be addressed is whether fine modulation could also be observed SMR in metallic heterostructures. In this context, this study focuses on understanding the importance of Néel vector in $IrMn_3$ for improved tunability of the SMR effect in NiFe\$IrMn_3$\Pt metal layers.

2. Experimental

The $IrMn_3$ thin films were fabricated using UHV-MBE co-evaporation technique at room temperature (RT) by controlling the relative deposition rate between Ir and Mn. Ir and Mn were deposited at a base pressure of 2.2×10^{-10} Torr with a deposition rate of 0.02 nm/s and 0.06 nm/s for Ir and Mn, respectively, at RT. Before depositing $IrMn_3$ films, a 1.5-nm-thick layer of NiFe was first deposited on Si(100)\SiO_2 substrates using UHV-MBE at RT, at a deposition rate of 0.03 nm/s, and a base pressure of 3.9×10^{-10} Torr.

Pt-based Hall devices of NiFe\$IrMn_3$\Pt structures were prepared by UHV-MBE using shadow masking techniques, with a deposition rate of 0.016 nm/s, and at a base pressure of 1.2×10^{-10} Torr. The thickness of the Pt films was kept within the spin diffusion length of Pt and minimized down to the experimental limit, where the films formed continuous and conductive layers (3.0 nm-thick). The electrical characterization was performed in a variable-temperature probe station using nitrogen cooling down to 77 K, with magnetic fields up to 8 kG. A Keithley 6220 was used as a current source, and a Keithley 2182A as a nanovoltmeter. The angular dependent magnetoresistance (ADMR) measurements were performed in a Quantum Design physical property measurement system with an in-built low-frequency alternate-current lock-in board. For all cases, standard four-probe measurement schemes were used. The current, I, was injected along the Hall bar. Following a right-hand rule, we defined the x-axis parallel to the current injection path, the z-axis perpendicular to the film surface, and the y-axis perpendicular to both.

The surface morphology of $IrMn_3$ films was also carefully analyzed using AFM to optimize the film growth condition. A SQUID magnetometer also characterized magnetic properties.

3. Results and Discussion

The temperature dependence of the resistivity, ρ, of NiFe\3.0 nm $IrMn_3$\Pt and 3.0 nm $IrMn_3$\Pt Hall bars was shown in Fig. 1(a). NiFe\3.0 nm $IrMn_3$\Pt shows a metallic temperature dependence, while $IrMn_3$\Pt reveals a monotone increase as T decreases. Note that NiFe\Pt bilayer prepared under the same growth condition using the same film deposition technique typically shows a metallic temperature dependence. The result was reported in our earlier study [12]. The middle panel in Fig. 1(a) presents the observation of AF phase transition of $IrMn_3$ thin films in NiFe\$IrMn_3$\Pt structures. Using the same method, we employ to determine Néel temperature in ultrathin Mn films, the Néel temperature is determined [13]. The bulk $IrMn_3$ is well-known as a high magnetic transition temperature $T_N \sim 950$ K [14]. However, finite-size effects in thin films lead to the deviation of the magnetic and transport properties from those of bulk samples [15]; we observe the Néel point to be at $T_N \sim 197$ K for 3.0 nm $IrMn_3$ thin film, which agrees with the literature reported $IrMn_3$ thin film [16, 17].

We observe the existence of exchange coupling between NiFe and $IrMn_3$ at 77 K. As shown in Fig. 1(b), the coercivity field of 160 G is about two times of magnitude larger than that of NiFe thin films (~ 80 G) [18]. Our results are in agreement with the previous results reported in Refs [19, 20]. Therefore, the exchange coupling between the Néel vector ($\mathbf{\Delta} = \boldsymbol{M}_\mathbf{A} - \boldsymbol{M}_\mathbf{B}$) of $IrMn_3$ and the magnetization of NiFe becomes essential and influences the spin transport across the NiFe\$IrMn_3$ and $IrMn_3$\Pt interface. The magnetic moment curves reveal that the easy magnetic axis is along the in-plane direction (x-axis), while the hard axis is along the out-of-plane direction (z-axis). The saturation magnetization is not reached when H applies along the z-axis. Fig. 1(c) shows the surface morphology of 3.0 nm $IrMn_3$ film grown on 1.5 nm NiFe. The AFM result shows a smooth surface (RMS roughness ~ 0.20 nm). The smooth surface morphology of $IrMn_3$

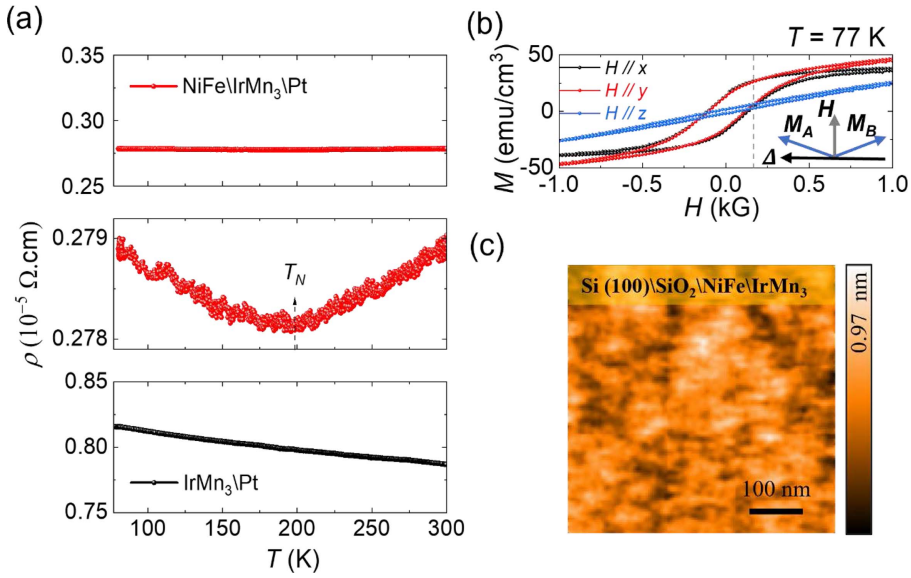

Figure 1. Electrical & magnetic properties and surface morphology of the sample NiFe\IrMn$_3$\Pt. (a) Temperature dependence of resistivity, $\rho(T)$, of sample NiFe\IrMn$_3$\Pt (top panel) with reference sample without NiFe layer (lower panel). The middle panel is the enlarged $\rho(T)$ result of sample NiFe\IrMn$_3$\Pt. The Néel temperature, T_N, is of ~ 200 K. (b) Magnetic hysteresis loops at 77 K, below T_N, for sample NiFe\IrMn$_3$\Pt with the external magnetic field applied parallel to *x*-, *y*-, and *z*-directions. The coercivity value is approximately 160 G, shown as the dashed grey line. (c) AFM image (0.5 μm×0.5 μm) of the surface morphology for sample NiFe\IrMn$_3$\Pt with the root mean square (RMS) roughness is ~0.2 ± 0.0 nm.

thin films benefits a further study of IrMn$_3$-based SMR.

We performed ADMR measurements as a function of representative magnetic field (2, 4, 6, 10, and 20 kG) at T = 77 K as presented in Fig. 2. Focusing on α-angle, Fig. 2(a), the angular dependence varies in the *x*-*y* plane. The resistivity shows a minimum when $\alpha = 0°$ (H // y) and $\alpha = 180°$ (H //-*y*) and a maximum when $\alpha = 90°$ (H // *x*) and $\alpha = 270°$ (H //-*x*), both the conventional AMR and SMR contribute to the overall MR. The magnitudes of AMR increase with increasing the magnitude of the external magnetic field. For β-angle, Fig. 2(b), the angular dependence varies in the *y*-*z* plane, which supports the existence of SMR. Given this, we can say that the spin current generated in Pt can transport through IrMn$_3$ and interact with NiFe. This result implies that the spin current can propagate in the long-range order within the 3.0 nm IrMn$_3$ layer. Interestingly, the sign of MR changes when the applied magnetic field increases up to 6 kG. For γ-angle, Fig. 2(c), the resistance changes with increasing the amplitude of the applied field in the *x*-*z* plane, indicating the existence of AMR. The MR signals in trilayers of NiFe\IrMn$_3$\Pt are governed by the magnetic properties in IrMn$_3$ layer. Table 1 shows the collection of the measured MR values of NiFe\IrMn$_3$\Pt in applying different magnetic field at 77 K, which corresponds to the ADMR results in Figure 2.

The magnetization in NiFe is easily aligned with the direction of the applied field due to its soft magnetic behavior. Applying magnetic field along the easy axis, higher than the spin-flop field (H_{SF}), the Néel vector will be changed with its direction perpendicular to H, called the spin-flop transition [21]: see Fig. 3.

Table 1. Summary of the MR ratio of sample NiFe\IrMn$_3$\Pt at 77 K, below the Néel temperature, for various magnitudes of the external magnetic field.

	MR ratio (10^{-4})		
H (kG)	Θ_{xy} [$(R_x - R_y)/R_y$]	Θ_{yz} [$(R_z - R_y)/R_y$]	Θ_{xz} [$(R_x - R_z)/R_z$]
2	3.40	3.58	0
4	5.61	1.43	3.11
6	4.87	0	4.79
10	6.80	-2.15	7.67
20	6.24	-3.80	9.47

In applying H < 6 kG, the IrMn$_3$ moments can be frustrated but remains along the easy axis. Some IrMn$_3$ moments could still be parallel to spin polarization in Pt, and the spin current is reflected at the interface of IrMn$_3$\Pt. On the other hand, there can exist the remaining IrMn$_3$ moments perpendicular to spin polarization in Pt; the spin current can be absorbed at the interface of IrMn$_3$\Pt, which can transport through the IrMn$_3$ layer and interact with NiFe moments. Therefore, the positive SMR (~ $\cos^2\theta$) at H < 6 kG could reveal.

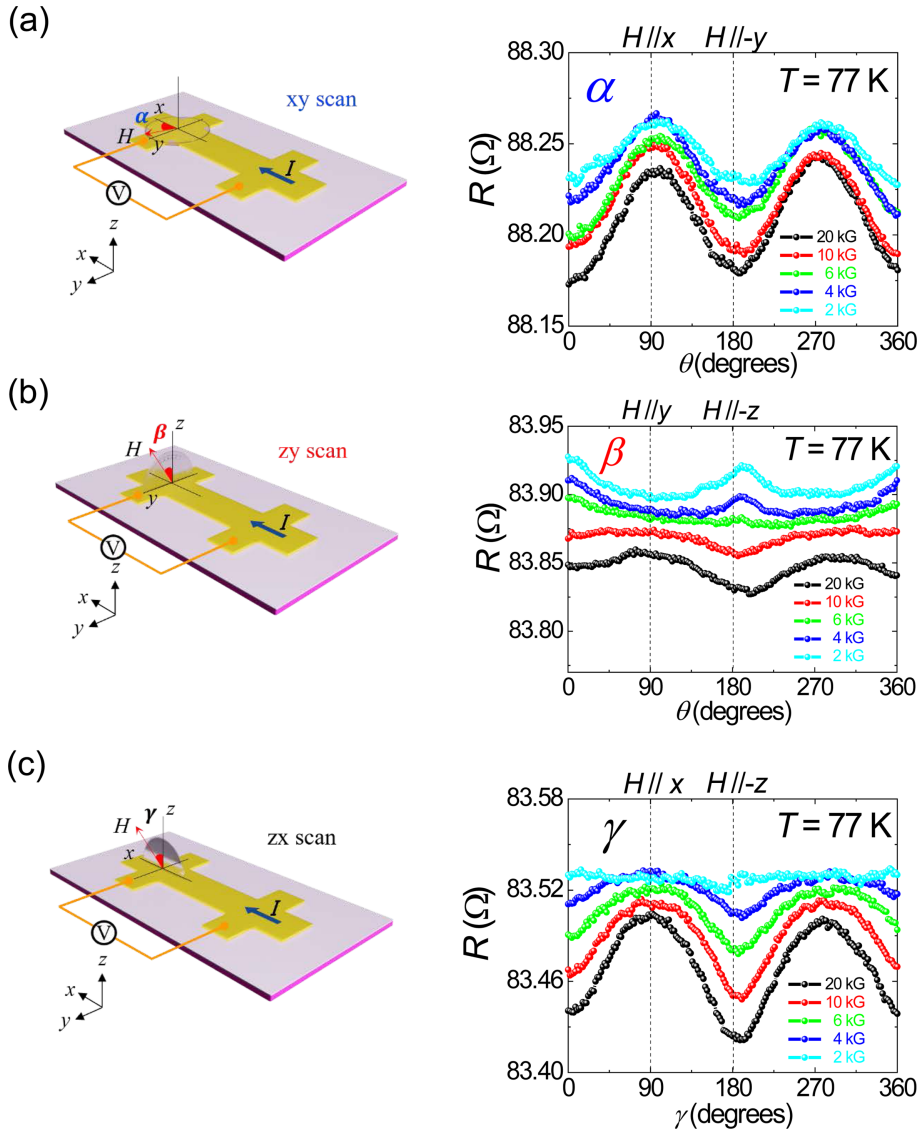

Figure 2. Angular dependent magnetoresistance (ADMR) results. ADMR of sample NiFe\IrMn$_3$\Pt measured under various external magnetic fields H = 2, 4, 6, 10, and 20 kG for (a) α, (b) β, and (c) γ-scans. All the data were recorded at T = 77 K.

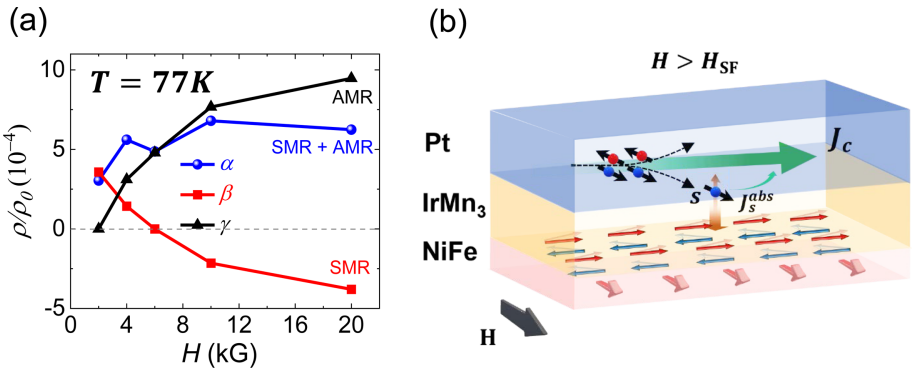

Figure 3. Schematics for SMR in our heterostructure. (a) The external magnetic field dependence of MR signals of α, β, γ- scans for sample NiFe\IrMn$_3$\Pt, at 77 K. (b) Illustration of the magnetic structure and spin transport in FM (FM = NiFe)\AFM (AFM = IrMn$_3$)\NM (NM = Pt) heterostructures the higher amplitude of the applied field compared to the spin-flop field.

In contrast, as increasing the external magnetic field H > 6 kG (see Fig. 3(b)), the spin-flop transition can occur in $IrMn_3$ layer. Thus, the Néel vector in $IrMn_3$ layer tends to orient perpendicular to the magnetic field as well as the magnetic moment of the NiFe layer. Given these, the SMR changes into the $\cos^2(90\text{-}\theta) = \sin^2\theta$ dependence in the y-z scan (β-scan). These observations imply the easy axis in $IrMn_3$ along the y-axis. This hypothesis goes in line with the y-easy axis in $IrMn_3$, which is determined by measuring the temperature dependence of the resistance of Pt Hall bars cooled under an external magnetic field (see Fig. 1(c)). When the external magnetic field is not parallel to the y-easy axis, the spin-flop transition is absent with increasing the magnitude external field, which means the y-component of the Néel vector can be slowly suppressed, resulting in dominantly AMR in x-z scans (γ-scans). The AMR and SMR simultaneously contribute to α-scans because both depend on the orientation of moments in the x-y plane [22].

The AF $IrMn_3$ can play a crucial role as a transmitter layer in the NiFe\$IrMn_3$\Pt trilayer devices. The generated spin current in the Pt layer can transport through the $IrMn_3$ layer, and interact with the NiFe layer. Therefore, the long-range transport of spin current can occur at low temperatures (below Néel temperature) in the magnetic hybrid structure by inserting the antiferromagnetic $IrMn_3$ layer. The SMR signals in NiFe\$IrMn_3$\Pt trilayers are governed by the interplay between the direction of charge current and the Néel vector, which is coupled with the magnetization of the NiFe layer via exchange coupling. These results in the change of SMR sign. Further improving the quality of $IrMn_3$ thin films can enhance the Néel temperature close to room temperature. This is promising for the realization of SMR devices working at RT. Our results highlight that the generation and detection of spin currents can be controlled by modifying the structural and magnetic properties at interfaces in magnetic hybrid structures.

4. Conclusion

In this work, a thin AF $IrMn_3$ film ranging from 0 to 3 nm was inserted between 1.5 nm thick NiFe and 3.0 nm thick Pt film. Interestingly, the SMR of ~ 0.036 % is observed in NiFe\3.0 nm $IrMn_3$\Pt trilayer structures when the temperature decreases below Néel temperature of the $IrMn_3$ films, as shown in the first value of θ_{yz} (see Table 1). Moreover, we observe the strong dependence of SMR behavior on the magnetic properties of $IrMn_3$ thin films, and the exchange coupling occurs at the NiFe\$IrMn_3$ interface. The sign of SMR signals is changed from positive to negative magnitude as the applied magnetic field becomes higher than 6 kG. Our results highlight that the Néel vector direction under different external magnetic field directions is the key point to understanding the SMR behaviors of FM\AF\NM magnetic hybrid structures.

Acknowledgements

This work was supported by the National Research Foundation grants funded by the Korea government (MSIT) (No. NRF-2021RF1A1064031 and 2021K1A3A 1A32084663). S.Y.P. acknowledges also the KBSI support (grant No. C230210) for the PPMS measurement.

References

[1] P. Wadley, B. Howells, J. Železný, C. Andrews, V. Hills, Campion R. P., V. Novák, K. Olejník, F. Maccherozzi, S. S. Dhesi, S. Y. Martin, T. Wagner, J. Wunderlich, F. Freimuth, Y. Mokrousov, J. Kuneš, J. S. Chauhan, M. J. Grzybowski, A. W. Rushforth, K. W. Edmonds, B. L. Gallagher, and T. Jungwirth, Science **351**, 6273 (2016).

[2] H. Yan, Z. Feng, P. Qin, X. Zhou, H. Guo, X. Wang, H. Chen, X. Zhang, H. Wu, C. Jiang, and Z. Liu, Adv. Mater. **32**, 1905603 (2020).

[3] Y. T. Chen, S. Takahashi, H. Nakayama, M. Althammer, S. T. B. Goennenwein, Ei. Saitoh, and G. E. W. Bauer, Phys. Rev. B **87**, 144411 (2013).

[4] B. G. Park, J. Wunderlich, X. Martí, V. Holý, Y. Kurosaki, M. Yamada, H. Yamamoto, A. Nishide, J. Hayakawa, H. Takahashi, A. B. Shick, and T. Jungwirth, Nature Mater. **10**, 347 (2011).

[5] H. Reichlová, D. Kriegner, V. Holý, K. Olejník, V. Novák, M. Yamada, K. Miura, S. Ogawa, H. Takahashi, T. Jungwirth, and J. Wunderlich, Phys. Rev. B **92**, 165424 (2015).

[6] Y. Yang, Y. Xu, X. Zhang, Y. Wang, S. Zhang, R. W. Li, M. S. Mirshekarloo, K. Yao, and Y. Wu, Phys. Rev. B **93**, 094402 (2016).

[7] A. Manchon, Phys. Status Solidi RRL **11**, 1600409 (2017).

[8] W. Lin and C. L. Chien, Phys. Rev. Lett. **118**, 067202 (2017).

[9] D. Hou, Z. Qiu, J. Barker, K. Sato, K. Yamamoto, S. Vélez, J. M. Gomez-Perez, L. E. Hueso, F. Casanova, and E. Saitoh, Phys. Rev. Lett. **118**, 147202 (2017).

[10] Y. Yang, Y. Xu, K. Yao, and Y. Wu, AIP Adv. **6**, 065203 (2016).

[11] N. Nagaosa, J. Sinova, S. Onoda, A. H. MacDonald, and N. P. Ong, Rev. Mod. Phys. **82**, 1539 (2010).

[12] J. H. Park, M. Ribeiro, T. K. H. Pham, N. J. Lee, T. W. Eom, J. H. Jo, S. Y. Park, S. H. Rhim, K. Nakamura, J. W. Yoo, and T. H. Kim, J. Vac. Sci. Technol. B **38**, 040602 (2020).

[13] T. K. H. Pham, M. Ribeiro, and T. H. Kim, Thin Solid

Films **671**, 1 (2019).
[14] H. Chen, Q. Niu, and A. H. MacDonald, Phys. Rev. Lett. **112**, 017205 (2014).
[15] X. Y. Lang, W. T. Zheng, and Q. Jiang, Phys. Rev. B **73**, 224444 (2006).
[16] D. Petti, E. Albisetti, H. Reichlová, J. Gazquez, M. Varela, M. Molina-Ruiz, A. F. Lopeandía, K. Olejník, V. Novák, I. Fina, B. Dkhil, J. Hayakawa, X. Marti, J. Wunderlich, T. Jungwirth, and R. Bertacco, Appl. Phys. Lett. **102**, 192404 (2013).
[17] L. Frangou, S. Oyarzún, S. Auffret, L. Vila, S. Gambarelli, and V. Baltz, Phys. Rev. Lett. **116**, 077203 (2016).
[18] M. Romera, R. Ranchal, D. Ciudad, M. Maicas, and C. Aroca, J. Appl. Phys. **110**, 083910 (2011).
[19] X. Martí, B. G. Park, J. Wunderlich, H. Reichlová, Y. Kurosaki, M. Yamada, H. Yamamoto, A. Nishide, J. Hayakawa, H. Takahashi, and T. Jungwirth, Phys. Rev. Lett. **108**, 017201 (2012).
[20] F. Spizzo, M. Tamisari, F. Chinni, E. Bonfiglioli, and L. Del Bianco, J. Magn. Magn. Mater. **421**, 234 (2017).
[21] H. Wang, D. Hou, Z. Qiu, T. Kikkawa, E. Saitoh, and X. Jin, J. Appl. Phys. **112**, 083907 (2017).
[22] J. H. Han, C. Song, F. Li, Y. Y. Wang, G. Y. Wang, Q. H. Yang, and F. Fan, Phys. Rev. B **90**, 144431 (2014).